Chem. Chem. Technol., 2025, Vol. 19, No. 3, pp. 434–446 Chemistry

PORE STRUCTURE AND ADSORPTION PROPERTIES OF COAL-BASED ACTIVATED CARBONS PREPARED BY THERMALSHOCK ALKALINE ACTIVATION

Viktoriia Sabierova^{1, *}, Yuliia Tamarkina¹, Volodymyr Kucherenko¹

https://doi.org/10.23939/chcht19.03.434

Abstract. The adsorption of phenol, 4-chlorophenol, methylene blue, and Pb(II) by coal-based activated carbons prepared by a thermal shock alkaline activation was studied for the first time. The adsorption kinetics and isotherms were measured and compared with those of carbons obtained by a temperature-programmed activation. The adsorption rate was determined to be limited by the interaction of adsorbate with surface centers, and not by the diffusion into pores. Thermal shock increases adsorption rates by 1.18-3.16 times and equilibrium capacities by 1.13-2.08 times, depending on the adsorbate and the coal type. The carbons prepared by thermal shock were found to be more effective adsorbents for water purification from ecotoxicants.

Keywords: coal, alkaline activation, thermal shock, activated carbon, adsorption, ecotoxicant.

1. Introduction

Industrial development creates many environmental problems, in particular, pollution of aquatic environments with ecotoxicants such as organic dyes, phenolic compounds,² and heavy metals.³ They are highly toxic, carcinogenic, mutagenic, resistant to biodegradation and solar radiation, and dyes also negatively affect photosynthesis in ecosystems. Among many methods of water purification,⁴ adsorption is the most common method of capturing ecotoxicants due to the relative simplicity of the process. Its efficiency directly depends on the adsorbents used, a significant group of which are carbon materials such as charcoals, biochars^{3,5} and activated carbons (ACs).⁶⁻¹³ They are prepared from various carbonaceous raw materials (woods, coals, polymers, various types of biomass) by carbonization or activation with various reagents (H₂O, CO₂, KOH, H₃PO₄, and others).

Currently, the greatest attention is paid to the studies of two groups of carbon materials, namely biochars and ACs obtained by alkaline activation – thermochemolysis (700–900°C) of the starting material with KOH. Only this method results in the formation of ACs with the largest specific surface area. For example, the scientific literature describes the preparation of such ACs from asphalt $(3851 \text{ m}^2/\text{g})$,6 petroleum coke (3950 m²/g),⁷ biomass $(3977 \text{ m}^2/\text{g})$,8 $(\leq 4012 \text{ m}^2/\text{g})^9$ anthracite (4482 m²/g),¹⁰ and urea-formaldehyde resin (4547 m²/g).¹¹ These and similarly prepared carbons also have good adsorption properties and sometimes demonstrate unique adsorption capacity. For example, carbons from alkali activated oxidized coals have phenol capacities of 3.32 – 4.81 mmol/g, biomass-based carbons have 4chlorophenol capacities up to 6.71 mmol/g, 12 and carbon from carbonized leaves activated with KOH shows a methylene blue dye capacity of 13.07 mmol/g. 10

Large specific surface areas, developed nanoporous structure, and high electrical conductivity of ACs determine their applications as an electrode material of supercapacitors, 13 holders of hydrogen 14 or natural gas, 15 adsorbents for water purification from ecotoxicants and capture of greenhouse gases (CO₂).^{16,17} Such materials are usually prepared at large weight ratios of KOH/substrate $R_{KOH} = 2 - 5$ g/g. This is the main disadvantage of alkaline activation, causing technological and environmental difficulties in the utilization of large quantities of alkali during the AC isolation. Therefore, an important and urgent task is the reduction of the alkali amount while maintaining the main distinctive properties of the resulting ACs. A way to solve this problem is to change the heating mode of the starting material processed by alkali. When studying the alkaline activation of brown coal, it was found¹⁸ that thermal shock - rapid introduction of a sample into a reactor zone preheated to the activation temperature (800°C) allows obtaining carbon with a larger specific surface area ($\sim 1700 \text{ m}^2/\text{g vs} \sim 1000 \text{ m}^2/\text{g}$) at a small ratio of $R_{KOH} = 1$ g/g. Subsequent studies confirmed the same effect in the alkaline activation of different rank coals. It could be expected that the ACs prepared by a thermal shock

¹ L. M. Litvinenko Institute of Physical-Organic and Coal Chemistry, National Academy of Sciences of Ukraine, Kharkivske shose, 50, Kyiv 02155, Ukraine

^{*,} victoria.bondaletova@gmail.com

Ó Sabierova V., Tamarkina Yu., Kucherenko V., 2025

would have a higher adsorption activity due to more developed nanoporosity, and the porous structure characteristics of these materials would make them promising for application in adsorption processes.

The aim of the work is to study the adsorption properties of different types of activated carbons prepared by the thermal shock alkaline activation related to typical organic ecotoxicants and pollutants such as phenol, 4-chlorophenol, methylene blue, and lead cations, and to compare them with the properties of adsorbents obtained by conventional temperature-programmed alkaline treatment.

2. Experimental

2.1. Fossil Coals and Reagents

The original coal samples were brown coal (B) from the Aleksandriya deposit and long-flame coal (D) from the Donbass deposit. The particle size of coals is 0.16-0.25 mm; the proximate and elemental analyses are given in Table 1.

Potassium hydroxide (Chemapol, CAS 1310-58-3) was used as an activator. Methylene blue dye (Enamine Ltd.,

CAS 61-73-4), phenol (Enamine Ltd., CAS 108-95-2), and 4-chlorophenol (Enamine Ltd., CAS 106-48-9) were used as received. Lead nitrate (Honeywell Fluka, CAS 10099-74-8) in acetate buffer (pH 5.4) was used as a precursor of Pb(II) cations.

2.2. Preparation of Activated Carbons

The ACs preparation was carried out in two main stages: alkaline impregnation and activation – thermochemolysis in an inert environment. The impregnation with potassium hydroxide was performed by mixing dried coal (10 g) and a 30% aqueous solution of KOH (33.3 g) with the weight ratio KOH/coal $R_{KOH}=1.0~g/g$ and exposing for 24 h at room temperature. Then the aqueous phase was removed at $90-100^{\circ}\text{C}$ and the residue was dried at $110-130^{\circ}\text{C}$.

Activation was performed using two methods. The first one is a new method – the thermal-shock alkaline activation, abbreviated as TS-activation. A stainless steel reactor (diameter 40 mm, working area height 150 mm) was purged with dry argon (~2 dm³/h) and heated to a given thermal shock temperature (800°C). Then, impregnated coal was quickly introduced into the heated zone, held for 1 h, and quickly cooled in a flow of argon.

Table 1. Proximate and elemental analysis of coals

Coal	Proximate analysis, wt %			Elemental analysis, wt %					
	W ^a	A^d	V^{daf}	C ^{daf}	$\mathbf{H}^{\mathrm{daf}}$	S^{daf}	N ^{daf}	O ^{daf}	
Brown coal (B)	12.4	1.7	57.6	70.4	6.0	3.8	2.0	17.8	
Long-flame coal (D)	11.1	1.8	43.8	80.0	5.3	1.0	1.9	11.8	

The resulting product – a mixture of AC and potassium compounds (mostly KOH, K2CO3, K2O) was sequentially washed with water from alkali, then with an HCl aqueous solution (0.1 N), and again with water until the reaction to Cl⁻ ions was negative (qualitative test with AgNO₃). The resulting AC sample was dried at 120±10°C to constant weight, and the AC yield (Y, %) was determined. The same samples of impregnated coals were activated by a conventional temperature-programmed alkaline activation (TP-activation). It was performed in the same way as TS-activation, but heating to the final activation temperature (800°C) was carried out slowly at a rate of 4°C/min. Activated carbons prepared from brown coal were designated as AC(B)(TS) and AC(B)(TP); samples from long-flame coal were designated as AC(D)(TS) and AC(D)(TP).

2.3. Characterization of Activated Carbons

The characteristics of the AC porous structure were determined by isotherms of low-temperature (77 K)

nitrogen adsorption-desorption (Micromeritic ASAP 2020). The 2D-NLDFT-HS (2-Dimensional Non-local Density Functional Theory, Heterogeneous Surface) method¹⁹ (SAIEUS program) was used to calculate the integral and differential dependences of the S_{DFT} specific surface area (m^2/g) and the pore volume V (cm^3/g) from the average pore diameter (D, nm). The volumes of ultramicropores (V_{umi}), supermicropores (V_{smi}), subnanopores (V_{1nm}), and micropores (V_{mi}) were determined the integral dependences of V - D: $V_{mi} = V_{umi} + V_{smi}$. The total volume of meso- and macropores was calculated as $V_{me+ma} = V_t - V_{mi}$.

The specific surface areas of ultramicropores (S_{umi}), subnanopores (S_{1nm}), and micropores (S_{mi}) were taken from the integral dependence of S_{DFT} on D, calculated by 2D-NLDFT-HS method. The specific surface areas of the supermicropores (S_{smi}) and the total surface of meso- and macropores (S_{me+ma}) were calculated as $S_{smi} = S_{mi} - S_{umi}$ and $S_{me+ma} = S_{DFT} - S_{mi}$. The designation of pores and their average diameters were adopted in accordance with the IUPAC recommendation²⁰: ultramicropores (D \leq 0.7 nm), supermicropores (D \leq 0.7 nm), micropores

 $(D \le 2.0 \text{ nm})$. The above categories of pores were united by the term "nanopores" with an upper limit of $D \le 100 \text{ nm}$. The positive effect of thermal shock on the formation of AC porous structure was evaluated by the efficiency factor F(X) = X(TS)/X(TP), where $X = V_t$, V_{umi} , V_{smi} , V_{1nm} , V_{mi} , S_{DFT} , S_{umi} , S_{smi} , S_{1nm} , S_{mi} , S_{me+ma} .

2.4. Adsorption Measurements

Adsorption capacities of selected adsorbates A_{AD} (mmol/g), where AD is phenol (Ph), 4-chlorophenol (CPh), methylene blue (MB) or Pb(II) cations, were determined. The AC sample dried at $120\pm10^{\circ}$ C (m = 0.100 g) was placed in an Erlenmeyer flask, a volume ($V_{AD} = 100 \text{ cm}^3$) of the adsorbate aqueous solution with a given initial concentration (C_{AD(0)}, mmol/L) was added to the AC sample and shaken at 25±0.5°C (200 rpm, MAXTURDY-45 shaker bath, Daihan Scientific Co). In all experiments, the AC dosage in the adsorbate solution was constant, 1 g/L. After the specified time, the mixture was filtered, and the current concentration C_{AD} (during the adsorption kinetics measurement) or the equilibrium concentration C_{AD(e)} (during the adsorption isotherms registration) was measured. The concentrations of Ph, CPh, and MB were determined using calibration curves (absorbance vs concentration) at 270 nm, 280 nm, and 665 nm¹⁷, respectively (Perkin-Elmer Lambda 20 spectrophotometer). The concentration of Pb(II) cations was determined by titration with a trilon-B solution (0.005 M) in the presence of xylenol orange (0.05 wt %).22. The adsorption capacity A_{AD} was calculated as $A_{AD} = (C_{AD(0)} - C_{AD}) \times V_{AD}/m$. The specific adsorption capacity, $A_{AD(S)} = 1000 \times A_{AD(e)} / S_{DFT}$ (μmol/m²), was also determined, which is proportional to the surface concentration of adsorption centers.

Kinetic data for different adsorbates were obtained at the same initial concentration ($C_{AD(0)} = 5 \text{ mmol/L}$) and approximated by models of pseudo-first order (1), pseudo-second order (2) and intraparticle diffusion (3)^{23, 24}:

$$A_{AD} = A_{AD(e)} [1 - \exp(-k_1 \tau)]$$
 (1)

$$A_{AD} = k_2 A_{AD(e)}^2 \tau / (1 + k_2 A_{AD(e)} \tau)$$
 (2)

$$A = k_{d} \tau^{0.5} + C \tag{3},$$

where $A_{AD(e)}$ is the equilibrium adsorption capacity; k_1 , k_2 , k_d is the constants; τ is the adsorption time.

The initial adsorption rates ($R_{AD(0)}$, mmol/g·min) were calculated according to the following equation: $R_{AD(0)} = k_2 \cdot A_{AD(e)}^2$. Additionally, the adsorption capacity in the first minute of adsorption ($A_{AD(1)}$, mmol/g) was determined from the Eq. (2).¹² The initial adsorption activity of AC was determined by the portion (P, %) of the $A_{AD(1)}$ capacity in the equilibrium capacity and was calculated as $P = 100 \cdot A_{AD(1)} / A_{AD(e)}$.

The two-parameter models of Langmuir (4) and Freundlich (5) were used to approximate adsorption isotherms:²⁷

$$A_{AD(e)} = A_{AD(L)} k_{AJ(L)} C_{AD(e)} / (1 + k_{AD(L)} C_{AD(e)})$$
(4)

$$A_{AD(e)} = k_{AD(F)} \times C_{AD(e)}^{1/n}$$
 (5),

where $A_{AD(L)}$ is the adsorption capacity, which corresponds to a saturated adsorbate monolayer; $k_{AD(L)}$ is the constant of the Langmuir equation, $k_{AD(F)}$ and n are the constants of the Freundlich equation.

The effect of thermal shock on ACs adsorptive properties was evaluated by the efficiency factor F(Z) = Z(TS)/Z(TP), where $Z = A_{AD(e)}$, V_t , V_{umi} , V_{smi} , V_{1nm} , V_{mi} , S_{DFT} , S_{umi} , S_{smi} , S_{1nm} , S_{mi} , S_{me+ma} .

3. Results and Discussion

3.1. Selection of thermal-shock activation

The first work devoted to TS activation was carried out with demineralized $(A^d=0.5\%)$ brown coal impregnated with KOH. 18 Subsequent detailed studies showed the following: 26 a) with TS-activation (800°C), the reactivity of alkali metal hydroxides increases in the series LiOH<NaOH<KOH; b) at $R_{\rm KOH}=0.5-1.2~\rm g/g$, thermal shock increases $S_{\rm BET}$ values by 1.4–1.7 times (Table 2); c) the maxima of specific surface area and positive effect of thermal shock occurs when brown coal is activated at $R_{\rm KOH}=1.0~\rm g/g$ (Table 2); d) the optimal isothermal exposure time is 1 hour.

Table 2. Specific surface areas of ACs prepared from demineralized brown coal by TS-activation and TP-activation²⁶

A ativation mathed	R_{KOH} , g/g								
Activation method	0.2	0.5	0.8	1.0	1.2	1.5	2.0		
TS-activation	660	1210	1350	1700	1550	1160	970		
TP-activation	530	870	980	1000	1040	990	1030		

Under identical TS-activation conditions ($R_{KOH} = 1.0 \text{ g/g}$, 800°C), AC samples were prepared from different rank coals with carbon content within $C^{daf} = 70.4-95.6 \text{ wt } \% \text{ (Fig. 1).}^{18}$

The AC samples prepared by TS-activation are characterized by higher S_{DFT} values (Fig. 1, line 1) compared to AC samples formed by TP-activation (Fig. 1, line 2). This is most noticeable for low-rank coals: the

maximum value ($S_{DFT} = 2012 \text{ m}^2/\text{g}$) has the AC from brown coal, and very similar values ($S_{DFT} = 1950-1955 \text{ m}^2/\text{g}$) have the ACs from coals with $C^{daf} = 80-81 \text{ wt}$ %. The efficiency of thermal shock for increasing the specific surface area can be estimated by the efficiency factor $F(S_{DFT})$ as the ratio of $S_{DFT}(TS)/S_{DFT}(TP)$. With increasing the coal rank, the efficiency of thermal shock decreases towards middle rank coals (Fig. 1, line 3) and then sharply increases to a maximum under TS-activation of anthracite ($F(S_{DFT}) = 2.54$). Thermal shock shows the greatest development of the surface for low-rank coals. For this reason, two low-rank coals – brown coal (B) and long-flame coal (D) were selected for detailed studies.

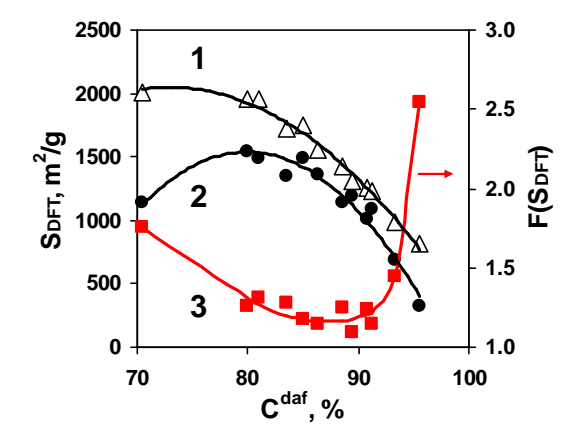


Fig. 1. Comparison of the specific surface area of ACs from different rank coals: (1) TS-activation, (2) TP-activation, (3) F(S_{DFT}) is the ratio of S_{DFT}(TS)/S_{DFT}(TP)

3.2. Pore structure

The nitrogen adsorption-desorption isotherms of ACs prepared are shown in Fig. 2. According to the IUPAC classification,²⁰ all isotherms are of type II with H4 type hysteresis. The shapes are similar and are the results of unrestricted monolayer-multilayer adsorption up to high relative pressure p/p₀. At low values of p/p₀, a sharp increase in the amount of adsorbed nitrogen indicates the dominance of microporosity. The beginning of the middle, almost linear section (called point B²⁰) corresponds to the completion of monolayer coverage. A more gradual curvature (i.e., a less distinctive point B) of the AC(B)(TS) isotherm is an indication of a significant amount of overlap of monolayer coverage and the onset of multilayer adsorption. When $p/p_0 \rightarrow 1$, the thickness of the adsorbed layer increases until the porous system is filled. Hysteresis is observed for all samples and appears due to the capillary condensation inside mesopores. It is more pronounced for ACs obtained by the thermal shock method. The common feature of hysteresis loops is the sharp step-down of the desorption branch at $p/p_0 = 0.4-0.5$, which is usually observed for nitrogen at a temperature of 77 K.

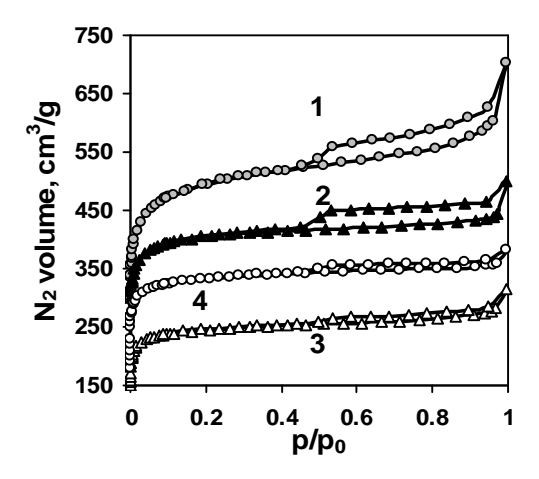


Fig. 2. Isotherms of nitrogen adsorption-desorption: 1) AC(B)(TS); 2) AC(D)(TS); 3) AC(B)(TP); 4) AC(D)(TP)

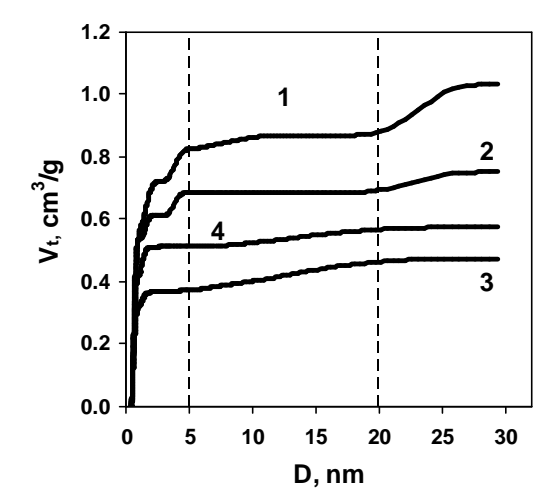


Fig. 3. Integral dependences of the total pore volume on pore diameter: 1) AC(B)(TS); 2) AC(D)(TS); 3) AC(B)(TP); 4) AC(D)(TP

The integral dependencies of the total pore volume V_t on the pore diameter (Fig. 3) show the following. The main shares of V_t values are volumes of pores with $D \le 5$ nm. Mesopores with D = 5 - 20 nm were developed slightly and were not developed in the AC(D)(TS) sample. The formation of pores with D = 20 - 30 nm almost does not occur during TP-activation, as can be seen from dependencies 3 and 4 in Fig. 3. In contrast, thermal shock forms mesopores with D = 20 - 30 nm, especially with TS-activation of brown coal (Fig. 3, line 1). The ACs prepared is characterized by a strong development of a microporous structure ($D \le 2$ nm), which can be seen from the initial sections of lines in Fig. 3. The volumes of different types of pores and the corresponding specific surface areas calculated from the dependences of V_t on D are

summarized in Table 3 and 4. The same characteristics of ACs prepared by TP-activation are also given there for comparison.

Comparing characteristics of the ACs prepared by the two activation methods shows the following. The AC yields under TS-activation are lower because of higher yields of volatile products due to their simultaneous pulsed formation during thermal shock. That is, thermal shock reduces the AC yield from brown coal by 1.30 times, and from long-flame coal by 1.15 times. At the same time, all porosity parameters were improved when replacing temperature-programmed heating with thermal shock. This confirms the higher efficiency of TS-activation in relation to the formation of the AC porous structure. The factors of

efficiency (F) are significantly higher for brown coal (Tables 3 and 4), that is, this coal is more sensitive to thermal shock compared to long-flame coal. A comparison of pore structure parameters of the AC(B)(TS) and AC(D)(TS), prepared from coals B and D under the same conditions of TS-activation, shows the following. The total pore volume of AC(B)(TS) is significantly (by $0.31~\rm cm^3/g$) larger than the V_t value in the AC(D)(TS) sample due to the larger volume of meso- and macropores (by $0.23~\rm cm^3/g$) and micropores (by $0.08~\rm cm^3/g$). This is due to the higher yield of volatile products from brown coal during its thermochemolysis with KOH, which leads to a lower yield of ACs and the formation of large pores in the AC spatial framework.

Table 3. Yields and different pore volumes of ACs prepared

Coal	Sample	Y, wt %	V _t , cm ³ /g	V _{umi} , cm ³ /g	V _{smi} , cm ³ /g	V_{1nm} , cm ³ /g	V _{mi} , cm ³ /g	V _{me+ma} ,cm ³ /g
	AC(B)(TS)	22.7	1.08	0.33	0.36	0.54	0.69	0.39
Brown coal (B)	AC(B)(TP)	29.5	0.49	0.22	0.15	0.32	0.37	0.12
(=)	F		2.20	1.50	2.40	1.69	1.86	3.25
Long-	AC(D)(TS)	43.4	0.77	0.41	0.20	0.54	0.61	0.16
flame	AC(D)(TP)	49.8	0.59	0.31	0.20	0.42	0.51	0.08
coal (D)	F		1.31	1.32	1.00	1.29	1.20	2.00

Table 4. Specific surface areas of different pores of ACs prepared

Coal	Sample	$S_{DFT}, m^2/g$	S_{umi} , m^2/g	S_{smi} , m^2/g	S_{1nm} , m^2/g	S_{mi} , m^2/g	S_{me+ma} , m^2/g
	AC(B)(TS)	2012	1153	753	1688	1906	205
Brown coal (B)	AC(B)(TP)	1142	793	327	1050	1120	22
	F	1.76	1.45	2.30	1.61	1.70	9.32
Long-flame coal (D)	AC(D)(TS)	1950	1470	433	1807	1903	47
	AC(D)(TP)	1547	1116	419	1401	1535	22
	F	1.26	1.32	1.03	1.29	1.24	2.14

The subnanopore volumes of both samples are the same but their shares in the total pore volume (V_{lnm}/V_t) differ and are ~50% for AC(B)(TS) and ~70% for AC(D)(TS). Subnanopores are now attracting special attention because they determine the abnormally large electrical capacity of supercapacitors, ^{27,28} high adsorption capacity for CO₂, ²⁹ the formation of adsorbed hydrogen layers with the liquid or solid densities, ¹⁴ the possibility of cations separation by size in the cyclic charge/discharge electrosorption. ³⁰ The AC(D)(TS) sample is also characterized by the dominance of ultramicropores: the V_{umi}/V_{smi} ratio is ~2.0 vs 0.9 for the AC(B)(TS). Pore volume variations also affect specific surface areas of different pores (Table 4). With almost equal

 S_{DFT} and S_{mi} values of both samples, the AC(D)(TS) has a subnanopores specific surface area 1.07 times larger, and an ultramicropores surface area 1.3 times larger compared to AC(B)(TS). Thus, during TS-activation of long-flame coal, active carbon is formed with more developed subnanoporosity due to the dominant formation of ultramicropores $(D \le 0.7 \text{ nm})$.

3.3. Adsorption measurements

3.3.1. Kinetics of adsorption

For all four AS samples, the adsorption kinetics of each adsorbate was measured at 25°C. For a unified

comparison of ACs adsorption activity, all kinetic curves were measured at the same initial concentration of selected adsorbates $C_{AD(0)} = 5$ mmol/L. As an illustration, Fig. 4 shows the adsorption kinetics by the AC(D)(TS) sample. The other samples show qualitatively the same pictures; the differences are only in the numerical values of the adsorption capacities. In all cases, adsorption equilibrium is reached for 2-4 hours, depending on the adsorbate nature. Kinetic data were approximated by models of pseudo-first order (1), pseudo-second order (2), and intraparticle diffusion (3). Adsorption kinetics of selected compounds was determined to be poorly approximated by the pseudo-first order model: determination coefficients vary within $R^2 = 0.648 - 0.991$.

Adsorption kinetics are more accurately approximated by the pseudo-second order model ($R^2 \ge 0.993$), according to which the solid lines in Fig. 4 were calculated. This model postulates that the rate of adsorption is limited by interaction of adsorbates with the surface adsorption centers,²³ and not by diffusion into the porous system of activated carbon. The maximum adsorption capacities

 $A_{AD(m)}$ and the constant k_2 were calculated by linearization in the coordinates " $(\tau/A_{AD}) - \tau$ " and given in Table 5.

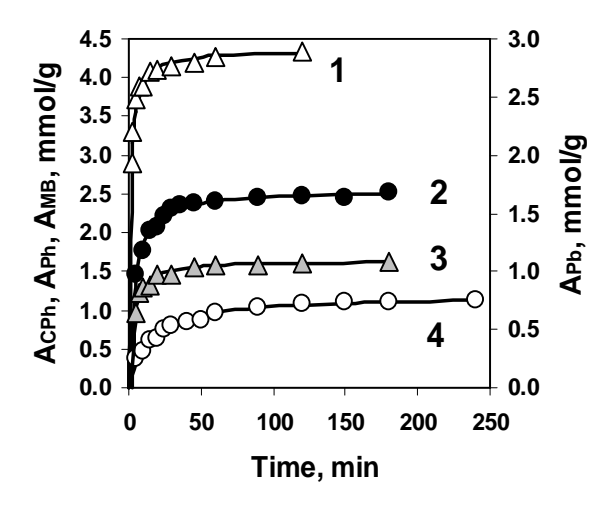


Fig. 4. Kinetics of adsorption by the AC(D)(TS) sample: 1 - CPh, 2 - Ph, 3 - Pb(II), 4 - MB

Table 5. Parameters of the pseudo-second order models for adsorption by AC samples

Commle	Parameter		Adsorbate					
Sample	Parameter	Ph	CPh	MB	Pb(II)			
	A _{AD(e)} , mmol/g	2.451	3.350	1.219	0.736			
	k ₂ ×10 ² , g/mmol⋅min	10.3	29.7	4.36	50.2			
AC(B)(TS)	R _{AD(0)} , mmol/g·min	0.619	3.333	0.065	0.272			
AC(B)(13)	A _{AD(1)} , mmol/g	0.495	1.672	0.062	0.199			
	$P = A_{AD(1)}/A_{AD(e)}$, %	20.2	49.9	7.5	27.0			
	$A_{AD(S)}$, μ mol/m ²	1.22	1.67	0.56	0.36			
	A _{AD(e)} , mmol/g	1.694	2.419	0.964	0.354			
	$k_2 \times 10^2$, g/mmol·min	9.95	37.4	5.96	69.0			
AC(D)(TD)	R _{AD(0)} , mmol/g·min	0.286	2.188	0.055	0.086			
AC(B)(TP)	A _{AD(1)} , mmol/g	0.244	1.148	0.028	0.070			
	$P = A_{AD(1)}/A_{AD(e)}$, %	4.9	23.0	0.55	1.39			
	$A_{AD(S)}$, μ mol/m ²	1.48	2.12	0.84	0.31			
	A _{AD(e)} , mmol/g	2.561	4.359	1.200	1.097			
	$k_2 \times 10^2$, g/mmol·min	9.81	20.31	5.56	30.97			
AC(D)(TS)	R _{AD(0)} , mmol/g·min	0.643	3.859	0.080	0.373			
AC(D)(TS)	A _{AD(1)} , mmol/g	0.514	2.050	0.075	0.278			
	$P = A_{AD(1)}/A_{AD(e)}$, %	20.1	47.0	6.3	25.3			
	$A_{AD(S)}$, μ mol/m ²	1.31	2.22	0.62	0.56			
	A _{AD(e)} , mmol/g	1.592	3.859	0.801	0.688			
	$k_2 \times 10^2$, g/mmol·min	13.08	19.82	5.15	43.38			
AC(D)(TP)	R _{AD(0)} , mmol/g·min	0.332	2.952	0.033	0.205			
AC(D)(IF)	$A_{AD(1)}$, mmol/g	0.274	1.669	0.032	0.158			
	$P = A_{AD(1)}/A_{AD(e)}$, %	5.48	33.4	0.63	3.16			
	$A_{AD(S)}$, μ mol/m ²	1.03	2.49	0.52	0.44			

Differences in rates of adsorption by AC samples are given by comparing the $R_{\rm AD(0)}$ values (Table 5). It is noteworthy that the higher adsorption capacities (by 1.36-2.42 times) and initial adsorption rates of chlorophe-

nol compared to phenol are observed. If we assume that the adsorption rate is determined by diffusion, one could expect lower rates of CPh adsorption since the size of CP molecules is larger and their transport into the AC

microporous structure is more difficult. The data obtained (Table 5) indicate the opposite: the CPh adsorption by all samples proceeds 5.38-8.89 times faster, judging by the comparison of the $R_{\text{CPh}(0)}$ and $R_{\text{Ph}(0)}$ values. This is additional confirmation that the rate of adsorption by AC samples is limited by interaction (physical sorption and chemisorption) with surface adsorption centers.

Adsorption kinetic data are often approximated with an intraparticle diffusion model (3) to identify the ratelimiting step. As an example, Fig. 5 shows the application of this model for adsorption by the AC(D)(TS) sample. Other samples show very similar pictures; the differences lie only in the numerical values of the coefficients, which are summarized in Table 6. This model assumes the following: 1) if diffusion into AC particles is the ratedetermining step, the dependence of the A_{AD} adsorption capacity on $\tau^{0.5}$ passes through the origin (C_{d1} = 0); 2) the presence of several linear sections indicates the presence of different adsorption mechanisms.²⁶ For AC samples prepared, the dependencies of A_{AD} on $\tau^{0.5}$ show two linear sections, and the first of them does not pass through the origin of coordinates ($C_{d1} > 0$). This confirms the absence of diffusion restrictions in the initial period of adsorption. It should be noted that the MB adsorption is characterized

by small values of C_{d1} (Table 6), so the rate of MB adsorption may be limited by diffusion. In addition, compared to other adsorbates, MB molecules are significantly larger, which complicates their transport into the AC microporous structure. As for other adsorbates, there are no such transport restrictions.

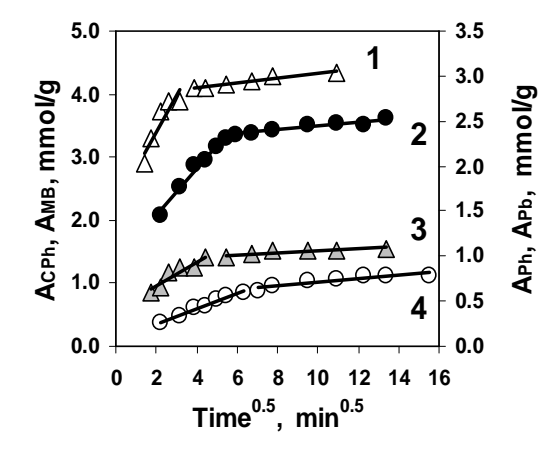


Fig. 5. Application of the intraparticle diffusion model for adsorption by the AC(D)(TS) sample: 1 - CPh, 2 - Ph, 3 - Pb(II), 4 - MB

TO 11 (D	C .1		1.00	1 1
Table 6.	Parameters	of the	intraparticle	diffusion	model

		Parameter								
Sanple	Adsorbate	k _{d1} , mmol/g∙min ^{0.5}	k _{d2} , mmol/g·min ^{0.5}	C _{d1} , mmol/g	C _{d2} , mmol/g	R^2_{d1}	R^2_{d2}			
	Ph	0.300	0.039	0.726	1.974	0.914	0.922			
A C(D)(TC)	CPh	0.244	0.019	2.230	3.120	0.965	0.89			
AC(B)(TS)	MB	0.127	0.034	0.060	0.651	0.976	0.901			
	Pb(II)	0.060	0.009	0.406	0.618	0.964	0.869			
	Ph	0.218	0.038	0.338	1.225	0.904	0.949			
AC(D)(TD)	CPh	0.307	0.017	1.243	2.224	0.952	0.984			
AC(B)(TP)	MB	0.076	0.016	-0.041	0.394	0.959	0.883			
	Pb(II)	0.037	0.005	0.142	0.282	0.979	0.876			
	Ph	0.256	0.021	0.937	2.232	0.973	0.916			
AC(D)(TC)	CPh	0.570	0.038	2.265	3.941	0.857	0.945			
AC(D)(TS)	MB	0.123	0.027	0.107	0.751	0.985	0.818			
	Pb(II)	0.134	0.011	0.395	0.952	0.891	0.721			
	Ph	0.172	0.018	0.479	1.330	0.982	0.831			
AC(D)(TP)	CPh	0.481	0.034	1.973	3.461	0.946	0.992			
AC(D)(TP)	MB	0.088	0.015	-0.048	0.490	0.965	0.866			
	Pb(II)	0.063	0.009	0.329	0.570	0.979	0.903			

3.3.2. Adsorption isotherms

Fig. 6 shows adsorption isotherms of the AC(B)(TS) sample from brown coal. Isotherms of other samples are of the same type and are not shown. Their approximation is performed by the Langmuir (4) and Freundlich (5) models, which are most often used for adsorption processes of selected adsorbates from aqueous

media. From the linearized forms of these models, the coefficients of the Langmuir equation (in the coordinates " $(C_{AD(e)}/A_{AD(e)}) - C_{AD(e)}$ ") and the Freundlich (in the coordinates " $lnA_{AD(e)} - lnC_{AD(e)}$ ") were calculated and summarized in Table 7.

The Langmuir model postulates that the AC surface is chemically homogeneous and the maximum adsorption capacity $(A_{AD(L)})$ corresponds to a saturated monolayer of

the adsorbate. The Freundlich model predicts a multilayer adsorption on a chemically heterogeneous surface that contains adsorption centers of different activity. The coefficient 1/n takes into account the surface heterogeneity, which is expressed in different values of the interaction energy between AC and adsorbate molecules. Under the condition 0 < 1/n < 1, the adsorption is favorable; when 1/n > 1, the adsorption process is unfavorable.²⁵ Both models are suitable for describing the adsorption isotherms of coal-based carbons prepared. Adsorption by AC samples obtained by TP-activation is better described by the Langmuir model $(R^2 = 0.986 - 0.998)$ compared to the Freundlich one $(R^2 = 0.908 - 0.984)$. As for the AC samples obtained with thermal shock, the Freundlich model approximates their isotherms with larger coefficients of determination: $R^2 = 0.986 - 0.998$ vs $R^2 = 0.981 - 0.994$. This is probably a consequence of the fact that the AC(B)(TS) and AC(D)(TS) samples have a more heterogeneous surface due to the pulsed ("explosion-like") formation of volatile products during the thermal shock.

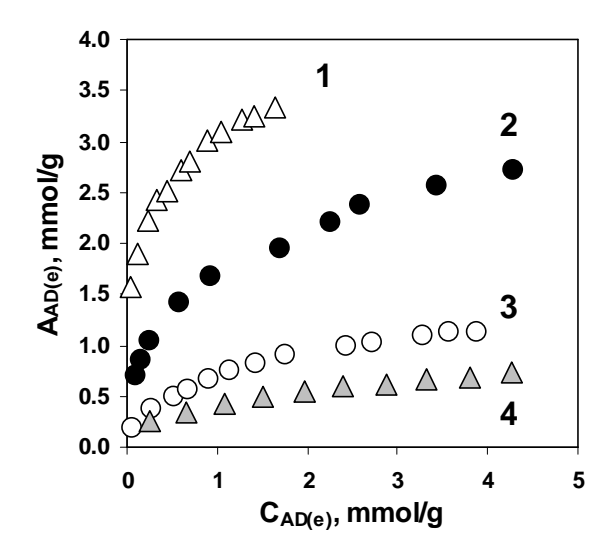


Fig. 6. Adsorption isotherms of the AC(B)(TS) sample: 1 - CPh, 2 - Ph, 3 - Pb(II), 4 - MB

Table 7. Parameters of the adsorption isotherms models of Langmuir and Freundlich

G 1	24.11	D		Adsorbate					
Sample Model		Parameter	Ph	CPh	MB	Pb(II)			
		A _{AD(L)} , mmol/g	2.965	3.514	1.337	0.933			
	Langmuir	k _{AD(L)} , L/mmol	1.76	7.67	1.28	0.82			
AC(D)(TS)		\mathbb{R}^2	0.990	0.994	0.987	0.993			
AC(B)(TS)		k _{AD(F)} , (mmol/g)(L/mmol) ^{1/n}	1.65	3.03	0.67	0.42			
	Freundlich	1/n	0.348	0.207	0.435	0.353			
		\mathbb{R}^2	0.994	0.998	0.995	0.986			
		A _{AD(L)} , mmol/g	1.850	2.560	1.139	0.447			
	Langmuir	k _{AD(L)} , L/mmol	3.63	5.75	0.30	0.52			
AC(D)(TD)		\mathbb{R}^2	0.998	0.998	0.986	0.989			
AC(B)(TP)	Freundlich	k _{AD(F)} , (mmol/g)(L/mmol) ^{1/n}	1.18	2.05	0.246	0.145			
		1/n	0.308	0.229	0.726	0.513			
		\mathbb{R}^2	0.967	0.969	0.984	0.908			
		A _{AD(L)} , mmol/g	4.187	4.484	1.296	1.458			
	Langmuir	k _{AD(L)} , L/mmol	0.66	22.30	1.45	0.76			
AC(D)(TC)		\mathbb{R}^2	0.987	0.994	0.981	0.988			
AC(D)(TS)		k _{AD(F)} , (mmol/g)(L/mmol) ^{1/n}	1.64	4.94	0.69	0.62			
	Freundlich	1/n	0.423	0.255	0.381	0.378			
		\mathbb{R}^2	0.995	0.997	0.995	0.993			
		A _{AD(L)} , mmol/g	2.967	3.952	0.998	0.921			
	Langmuir	A _{AD(L)} , mmol/g	2.967	3.952	0.312	0.543			
A C(D)(TD)		\mathbb{R}^2	2.967	0.998	0.986	0.993			
AC(D)(TP)		AC(D)(TP)	0.78	4.17	0.282	0.300			
	Freundlich	AC(D)(TP)	0.528	0.251	0.730	0.527			
		\mathbb{R}^2	0.984	0.918	0.986	0.913			

3.3.3. Comparison of different adsorbates

The highest adsorption capacity was found for the CPh adsorption, and the lowest for lead cations. The $A_{AD(e)}$ values of different adsorbates differ by 4.0-6.8 times and grow in a series Pb(II) < MB < Ph < CPh for all AC samples. The k_2 constants for all AC samples are the smallest for MB adsorption and increase in series MB < Ph < CPh < Pb(II). The k_2 values differ by 11.5 times for both ACs from brown coal and by 5.6 times for AC(D)(TS) and 8.4 times for AC(D)(TP). The measured values of $A_{AD(e)}$ (Table 5) are quite common. For comparison, the published capacities for adsorption of selected adsorbates by various types of carbon materials are below.

Phenol. Polymer-based ACs have capacities $A_{Ph(e)} \le 3.50 \text{ mmol/g.}^{31}$ The capacities of different-rank alkali-activated fossil coals ($R_{KOH} = 1 \text{ g/g}$, 800°C, 1 h) vary within $A_{Ph(e)} = 1.50 - 3.11 \text{ mmol/g}$, capacities from oxidized coals − within $A_{Ph(e)} = 3.32 - 4.81 \text{ mmol/g.}^{19}$

Chlorophenol. The A_{CPh(m)}values for different materials vary from 0.33 mmol/g (nanotubes) to 2.52 mmol/g (AC «Prolabo»).³² The AC samples prepared by KOH activation of organic wastes are characterized by capacities within 0.48 – 5.16 mmol/g.³³ There are reports of larger capacities: 5.62 mmol/g (coal-based active carbon, $S_{BET} = 1520 \text{ m}^2/\text{g})^{34}$ and even 6.71 mmol/g (biomass-based carbon, $S_{BET} = 1968 \text{ m}^2/\text{g})$.¹²

Methylene blue. The $A_{MB(e)}$ values of most carbon materials vary within $0.021-2.58~\text{mmol/g}.^{35-37}$ Materials with significantly higher adsorption capacity were also obtained, for example, $A_{MB(e)}=5.50-7.04~\text{mmol/g}$ of AC samples ($S=1814-2015~\text{m}^2/\text{g}$) prepared by biomass carbonization (450°C , 1 h) with subsequent alkaline activation ($R_{KOH}=3~\text{g/g}).^{38}$ Probably the largest capacity of MB ($A_{MB(e)}=4181.2~\text{mg/g}$ or 13.07~ммоль/r) was determined for the AC ($S=4482~\text{m}^2/\text{g}$) from carbonized lotus leaves activated with potassium hydroxide ($R_{KOH}=4~\text{g/g}).^{10}$ This value looks like the result of complete filling of the porous system with MB crystals, and not adsorption on the surface.

Pb(II) cations. The following capacities are given: 0.029-0.228 mmol/g (industrial carbons);³⁹ 0.064-1.42 mmol/g (nanotubes);⁴⁰ 0.029-1.731 mmol/g (biochars).⁴¹ The largest capacities are given for graphite oxide modified with polyaniline (6.834 mmol/g) and composite material from a mixture of iron oxide and reduced graphite oxide modified with sodium (8.04 mmol/g).⁴⁰

A comparison of the obtained (Table 5) and published data shows that the AC samples are characterized by fairly high adsorption capacities of all adsorbates. To a greater extent, this applies to the adsorption of phenolic

compounds, especially 4-chlorophenol. Judging by the $R_{AD(0)}$ values, the highest initial rate is observed for the CPh adsorption, the lowest for the MB adsorption. The difference in rates for different adsorbates is significant and equal to 48-51 times for both samples prepared by the thermal shock, and 44 and 89 times for other samples.

The ACs initial adsorption activities determined by the portion $P = 100 \cdot A_{AD(1)} / A_{AD(e)}$ differ for adsorptions of various adsorbates. From the data of Table 5, the minimum initial activities of AC samples is shown in the MB adsorption: P = 6.3 - 7.5% for AC(B)(TS) and AC(D)(TS)and 0.55 - 0.63% for AC(B)(TP) and AC(D)(TP). The highest initial efficiency is observed during the CPh adsorption: from 23% to ~50% of the maximum equilibrium quantity of chlorophenol is adsorbed in the first minute of the process. The $A_{AD(L)}$ values (Table 7) correspond to the saturated layer differ for adsorbates by 3.5 - 5.7 times, and for all AC samples grow in the same series as the $A_{AD(e)}$ values. Values of $A_{AD(L)}$ are larger than A_{AD(e)} values in all experiments. The closest values of A_{AD(L)} and A_{AD(e)} are determined for CPh adsorption, that is, the pseudo-second-order model and the Langmuir one give almost identical capacities.

3.3.4. The efficiency of thermal shock compared to temperature-programmed heating

The effect of thermal shock on the AC adsorption properties was evaluated by the factor F(Z) = Z(TS)/Z(TP), where $Z = A_{AD(e)}$, $A_{AD(L)}$, $A_{AD(S)}$, $A_{AD(1)}$, $R_{AD(0)}$, and $P = A_{AD(1)}/A_{AD(e)}$.

Thermal shock increases the equilibrium adsorption capacity in all cases, i.e., $F(A_{AD(e)}) > 1$ for all adsorbates (Table 8). The capacities of saturated adsorbate layers calculated from the Langmuir model also increase almost proportionally. The values $F(A_{AD(L)})$ and $F(A_{AD(e)})$ are quite close except for the adsorption of MB by AC samples from long-flame coal.

The values of factors $F(A_{AD(e)})$ and $F(A_{AD(L)})$ are individual for each adsorbed substance and depend on the type of the initial coal. The greatest effect of thermal shock is observed in the adsorption of Pb(II) cations. If the increase in adsorption capacity was caused only by an increase in the specific surface area (Table 4), then all values of $F(A_{AD(S)})$ would be equal to one. But this condition is not met. In half of the experiments, the efficiency factors are $F(A_{AD(S)}) > 1$, and this means an increase in the surface concentration of adsorption centers due to the replacement of temperature-programmed heating with the thermal shock. Other cases show $F(A_{AD(S)}) < 1$, therefore, the thermal shock reduces the number of these centers. Moreover, the effect of thermal

shock on the AC adsorption centers is sometimes opposite for ACs from different fossil coals. For example, for AC from long-flame coal, the thermal shock increases the number of surface centers being active regarding the phenol and MB, and for AC from brown coal, thermal shock reduces these parameters.

Coal	Adsorbate	Efficiency factor F for the parameter						
	Ausorbate	A _{AD(e)}	$A_{AD(L)}$	$A_{AD(S)}$	$R_{AD(0)}$	$A_{AD(1)}$	P	
	Ph	1.45	1.60	0.82	2.16	2.03	4.1	
Brown	CPh	1.38	1.37	0.79	1.52	1.46	2.2	
coal (B)	MB	1.26	1.17	0.67	1.18	2.21	13.6	
	Pb(II)	2.08	2.09	1.16	3.16	2.84	19.4	
Long-flame coal (D)	Ph	1.61	1.41	1.27	1.94	1.88	3.7	
	CPh	1.13	1.13	0.89	1.31	1.23	1.4	
	MB	1.50	1.01	1.19	2.42	2.34	10.0	
	Dh/II)	1 50	1.58	1 27	1.82	1.76	8.0	

Table 8. The efficiency factors of thermal shock compared to temperature-programmed activation

The AC samples prepared by TS-activation are characterized by an increased initial adsorption rate (Table 5). This is true for all adsorbates and AC samples, and the efficiency factors are $F(R_{AD(0)}) > 1$ (Table 8). The type of original coal also influences the $F(R_{AD(0)})$ value. For AC from brown coal, the thermal shock has the weakest effect on the initial adsorption of MB, and the strongest effect on the initial adsorption of Pb(II), which increases by more than 3 times. The degree of such influence increases in the series of adsorbates MB<CPh<Pb(II). Carbons from long-flame coal show a different sequence of adsorbates, namely CPh<Pb(II)<

Thermal shock has the greatest impact on the parameter $P = A_{AD(1)}/A_{AD(m)}$, which characterizes the ACs initial adsorption activities. This property of ACs is greatly improved by using thermal shock instead of temperature-programmed heating, especially for the adsorption of MB and lead cations (Table 8). It is also influenced by the type of initial coal, the AC precursor.

3.3.5. Comparison of the ACs prepared from brown coal and long-flame coal by TS-activation

Since the adsorption properties of ACs prepared by TS-activation were studied for the first time, it seemed appropriate to compare the characteristics of these carbons obtained from brown coal and long-flame coal. Comparison of parameters of the pseudo-second order model (Table 5) for these samples shows the following.

The capacities for phenol and MB are practically the same; the constants k_2 are close. The AC(D)(TS) sample adsorbs a larger quantity of CPh (1.3 times); the constant k_2 is 1.5 times larger. The same sample adsorbs a larger quantity of lead cations (by 1.2 times), although the constant k_2 is smaller (by 1.6 times). For all adsorbates, the specific adsorption capacities $A_{AD(S)}$ of the AC(D)(TS)

sample exceed those of the AC(B)(TS) sample. The values of such excess are small for phenol and MB adsorptions (≤ 1.11) , but for other adsorbates they are larger: 1.33 (CPh) and 1.56 (Pb(II)). The higher concentration of adsorbed substances CPh and Pb(II) on the AC(D)(TS) surface indicates additional routes of interacting adsorbate molecules with surface centers, which shifts the adsorption equilibrium. It is also likely that AC(D)(TS) has an additional number of centers which are active only toward CPh and Pb(II). This may be a consequence of the structural differences between the two carbons, in particular, the different number of phenolic and carboxyl groups involved in ion exchange reactions with lead cations. Another difference may be the different content and steric accessibility of graphene fragments of the AC spatial structure, which are responsible for the π -sorption of CPh and Pb(II) cations. 35,42

Based on the $R_{AD(0)}$ values, the initial adsorption rate by the AC(D)(TS) sample for all adsorbates is 1.04-1.37 times larger than that of the AC(B)(TS) from brown coal. This increase in the initial rate is small and is most likely due to the topochemical differences between the two carbon materials. The type of original coal has almost no effect on AC initial adsorption activities defined by the parameter $P = A_{AD(1)}/A_{AD(e)}$ (Table 5).

The adsorption isotherms of ACs from brown and long-flame coal (Table 7) are described by the Langmuir and Freundlich models in approximately the same way. The values of the saturated adsorbate layer $A_{AD(L)}$ increase for different substances by 3.5-3.8 times. For the AC(B)(TS) sample, these values increase in the series of adsorbates Pb(II) < MB < Ph < CPh. The same series is performed for the $k_{AD(L)}$ constants of this sample. For the AC(D)(TS) sample from long-flame coal, a different series of $k_{AD(L)}$ values was found as Ph < Pb(II) < MB < CPh, with the lowest constant for phenol adsorption $(k_{Ph(L)} = 0.66 \ L/mmol)$. The $k_{AD(L)}$ constants for the AC(B)(TS)

sample differ by 9.4 times for different adsorbates, and by 33.8 times for AC(D)(TS) due to the large value of the chlorophenol constant ($k_{CPh(L)} = 22.3$ L/mmol). Thus, the adsorption activity of the AC(D)(TS) is more sensitive to the adsorbate nature. It is characterized by higher adsorption capacities for all studied adsorbates. In addition, it has a more developed subnanoporous structure (Tables 2 and 4) and approximately 2 times higher yield. Since the total surface areas and micropore surface areas of both carbons are almost equal, the AC(D)(TS) sample is more effective as an adsorbent than the AC(B)(TS) sample from brown coal.

4. Conclusions

The adsorption of phenol (Ph), 4-chlorophenol (CPh), methylene blue (MB) dye, and Pb(II) cations by new activated carbons (ACs) prepared from brown coal and long-flame coal in a new process – thermal-shock alkaline activation was studied for the first time. The characteristics of the porous structure and adsorption activity of ACs are compared with the same characteristics of carbons obtained by the well-known method, temperature-programmed alkaline activation.

The use of thermal shock instead of temperature-programmed heating reduces the AC yields, but increases the total pore volume (by $1.31-2.20\,\mathrm{times}$) and the specific surface area (by $1.26-1.76\,\mathrm{times}$) due to the increase in the surface of micropores (D \leq 2.0 nm). Compared to brown coal, long-flame coal forms active carbons with more developed subnanoporosity due to the dominant formation of ultramicropores (D \leq 0.7 nm).

The kinetics of adsorption from aqueous solutions (25°C) is more accurately approximated by the pseudosecond order model ($R^2 \ge 0.993$) than by the pseudo-first order model ($R^2 \le 0.991$). Adsorption equilibria are reached in 2-4 hours, depending on the adsorbate nature. The adsorption rate is limited by the interaction of adsorbate molecules with surface adsorption centers, and not by diffusion into the AC porous structure. The initial rate, measured at the same initial concentration of 5 mmol/L, is the highest for the CPh adsorption (2.188 - 3.859 mmol/g·min), and the lowest is for the MB adsorption (0.033 – 0.080 mmol/g·min). The AC equilibrium capacity is the largest for the CPh adsorption (2.419 - 4.359 mmol/g), and the smallest is 0.3541.097 mmol/g for the Pb(II) adsorption. Thermal shock increases this rate by 1.18 - 3.16 times and the equilibrium capacity by 1.13 - 2.08 times, depending on the adsorbate and the type of fossil coal. Adsorption isotherms for all adsorbates are approximated by the Langmuir $(R^2 =$ = 0.981 - 0.994) and the Freundlich (R² = 0.986 - 0.998) models with close errors.

The thermal shock has the greatest impact on ACs initial adsorption activities, determined by the percentage of the substance adsorbed during the first minute. This property is greatly improved (by 1.4 - 19.4 times) due to the thermal shock, and is influenced by the type of initial coal, the AC precursor. Compared to ACs from brown coal, the AC from long-flame coal possesses higher adsorption capacities for all studied adsorbates, a more developed subnanoporous structure, and approximately 2 times higher yield. Since the total surface areas and micropore surface areas of both carbons are almost equal, the long-flame coalbased carbon has a greater adsorption ability. The ACs prepared by the thermal shock are more effective adsorbents for the purification of aquatic environments from ecotoxicants. Further research on coal-based activated carbons will focus on other practical applications, particularly as electrode materials for supercapacitors, adsorbents for storing natural gas and hydrogen, and for capturing carbon dioxide as a greenhouse gas.

Acknowledgements

The authors are grateful for the support provided by the National Academy of Sciences of Ukraine (Contract № 0117U000022). We thank Dr. Roman D. Mysyk, Basque Research and Technology Alliance (BRTA), Spain, for his help with adsorption measurements and calculations of low-temperature nitrogen adsorption isotherms.

References

```
[1] Oladoye, P.O.; Ajiboye, T.O.; Omotola, E.O.; Oyewola, O.J.
Methylene Blue Dye: Toxicity and Potential Elimination
Technology from Wastewater. Results Eng. 2022, 16, 100678.
https://doi.org/10.1016/j.rineng.2022.100678
[2] Garba, Z.N.; Zhou, W.; Lawan, I.; Xiao, W.; Zhang, M.;
Wang, L.; Chen, L.; Yuan, Z. An Overview of Chlorophenols as
Contaminants and their Removal from Wastewater by Adsorption:
A Review. J. Environ. Manage. 2019, 241, 59-75.
https://doi.org/10.1016/j.jenvman.2019.04.004
[3] Biswal, B.K.; Balasubramanian, R. Use of Biochar as a Low-
Cost Adsorbent for Removal of Heavy Metals from Water and
Wastewater: A Review. J. Environ. Chem. Eng. 2023, 11, 110986.
https://doi.org/10.1016/j.jece.2023.110986
[4] Nahurskyi, N.; Malovanyy, M.; Bordun, I.;
Szymczykiewicz, E. Magnetically Sensitive Carbon-Based
Nanocomposites for the Removal of Dyes and Heavy Metals from
Wastewater: A Review. Chem. Chem. Technol. 2024, 18, 170-
186. https://doi.org./10.23939/chcht18.02.170
[5] Pstrowska, K.; Łużny, R.; Fałtynowicz, H.; Jaroszewska, K.;
Postawa, K.; Pyshyev, S.; Witek-Krowiak, A.. Unlocking
Sustainability: A Comprehensive Review of Up-Recycling
Biomass Waste into Biochar for Environmental Solutions. Chem.
Chem. Technol. 2024, 18, 211-231.
https://doi.org/10.23939/chcht18.02.211
6
1
J
a
v
```

z m a

```
Area Porous Activated Carbon Derived from Asphalt. Carbon
2018, 140, 441-448. https://doi.org/10.1016/j.carbon.2018.08.038
[7] Mochizuki, T.; Kubota, M.; Matsuda, H.; D'Elia Camacho,
L.F. Adsorption Behaviors of Ammonia and Hydrogen Sulfide on
Activated Carbon Prepared from Petroleum Coke by KOH
Chemical Activation. Fuel Process. Technol. 2016, 144, 164-169.
https://doi.org/10.1016/j.fuproc.2015.12.012
[8] Liu, Z.; Hu, J.; Shen, F.; Tian, D.; Huang, M.; He, J.; Zou, J.;
Zhao, L.; Zeng, Y. Trichoderma Bridges Waste Biomass and Ultra-
High Specific Surface Area Carbon to Achieve a High-
Performance Supercapacitor. J. Power Sources. 2021, 497,
229880. https://doi.org/10.1016/j.jpowsour.2021.229880
[9] Hamyali, H.; Nosratinia, F.; Rashidi, A.; Ardjmand, M.
Anthracite Coal-Derived Activated Carbon as an Effectiveness
Adsorbent for Superior Gas Adsorption and CO2 / N2 and
CO<sub>2</sub> / CH<sub>4</sub> Selectivity: Experimental and DFT. J. Environ. Chem.
[10] Liu, G.; Qiu, L.; Deng, H.; Wang, J.; Yao, L.; Deng, L.
Ultrahigh Surface Area Carbon Nanosheets Derived from Lotus
Leaf with Super Capacities for Capacitive Deionization and Dye
Adsorption. Appl. Surf. Sci., 2020, 524, 146485.
Bttps://doi.org/10.1016/j.apsusc.2020.146485
Ol 1] Tiwari, D.; Bhunia, H.; Bajpai, P.K. Adsorption of CO<sub>2</sub> on
KOH Activated, N-Enriched Carbon Derived from Urea
Formaldehyde Resin: Kinetics, Isotherm and Thermodynamic
Studies. Appl. Surf. Sci. 2018, 439, 760-771.
https://doi.org/10.1016/j.apsusc.2017.12.203
[12] Wu, F.-C.; Wu, P.-H.; Tseng, R.-L.; Juang, R.-S. Preparation
Of Novel Activated Carbons from H2SO4-Pretreated Corncob
Hulls with KOH Activation for Quick Adsorption of Dye and 4-
Chlorophenol. J. Environ. Manage. 2011, 92, 708–713.
https://doi.org/10.1016/j.jenvman.2010.10.003
[13] Bora, M.; Bhattachariya, D.; Saikia, B.K. Coal-Derived
Activated Carbon for Electrochemical Energy Storage: Status on
Supercapacitor, Li-Ion Battery, and Li-S Battery Applications.
Energy Fuels 2021, 35, 18285-18307.
https://doi.org/10.1021/acs.energyfuels.1c02518
[14] So, S.H.; Lee, S.; Mun, J.; Rho, J.; Park, C.R. What Induces
the Dense Storage of Hydrogen of Liquid- or Solid-Like Density
Levels in Carbon Nanopores with sub-1 nm Diameters? Carbon
2023, 204, 594-600. https://doi.org/10.1016/j.carbon.2022.12.057
[15] Kumar, K.V; Preuss, K.; Titirici, M.-M.; Rodríguez-Reinoso,
F. Nanoporous Materials for the Onboard Storage of Natural Gas.
Chem. Rev. 2017, 117, 1796-1825.
https://doi.org/10.1021/acs.chemrev.6b00505
[16] Malini, K.; Selvakumar, D.; Kumar, N.S. Activated Carbon
from Biomass: Preparation, Factors Improving Basicity and
Surface Properties for Enhanced CO<sub>2</sub> Capture Capacity – A
Review. J. CO2 Util. 2023, 67, 102318.
https://doi.org/10.1016/j.jcou.2022.102318
[17] Zhao, C.; Ge, L.; Mai, L.; Li, X.; Chen, S.; Li, Q.; Li, S.;
Yao, L.; Wang, Y.; Xu, C. Review on Coal-Based Activated
Carbon: Preparation, Modification, Application, Regeneration,
and Perspectives. Energy Fuels 2023, 37, 11622-11642.
https://doi.org/10.1021/acs.energyfuels.3c01866
[18] Kucherenko, V.A.; Shendrik, T.G.; Tamarkina, Yu.V.;
Mysyk, R.D., Nanoporosity Development in the Thermal-Shock
KOH Activation of Brown Coal. Carbon 2010, 48, 4556-4558.
https://doi.org/10.1016/j.carbon.2010.07.027
[19] Jagiello, J.; Olivier, J.P. 2D-NLDFT Adsorption Models for
Carbon Slit-Shaped Pores with Surface Energetical Heterogeneity
```

```
and Geometrical Corrugation. Carbon 2013, 55, 70-80.
https://doi.org/10.1016/j.carbon.2012.12.011
[20] Thommes, M.; Kaneko, K.; Neimark, A. V.; Olivier, J.P.;
Rodriguez-Reinoso, F.; Rouquerol, J.; Sing, K.S.W. Physisorption
of Gases with Special Reference to the Evaluation of Surface Area
and Pore Size Distribution (IUPAC Technical Report). Pure Appl.
Chem. 2015, 87, 1051-1069. https://doi.org/10.1515/pac-2014-
1117
[21] Tamarkina, Yu.V.; Anishchenko, V.M.; Red'ko, A.M.;
Kucherenko, V.O. Aktyvovane luhom vykopne vugill'ya.
Mikroporysta struktura ta zdatnisť adsorbuvaty fenoľni spoluky.
Khimiya, Phisyka i Tekhnologiya Poverkhni. 2022, 13, 111-124.
https://doi.org/10.15407/hftp13.01.111
[22] Redko, A.V.; Tamarkina, Yu.V.; Redko, A.M.; Frolova, I.B.;
Kucherenko, V.O. Spriamovanist' zmin porystoi struktury i
adsorbtsiinoi zdatnosti pry topokhimichnomu okysneni
aktyvovanoho luhom vykopnoho vugill'ya. Pytannya Khimii
Khim. Tekhnol. 2023, 2, 127-136.
[23] Revellame, E.D.; Fortela, D.L.; Sharp, W.; Zappi, M.E.
Adsorption Kinetic Modeling Using Pseudo-First Order And
Pseudo-Second Order Rate Laws: A Review. Cleaner Eng.
Technol. 2020, 1, 100032.
https://doi.org/10.1016/j.clet.2020.100032
[24] Wang, J.; Guo, X. Rethinking of the Intraparticle Diffusion
Adsorption Kinetics Model: Interpretation. Solving Methods and
Applications. Chemosphere 2022, 309, 136732.
https://doi.org/10.1016/j.chemosphere.2022.136732
[25] Al-Ghouti, M.A.; Da'ana, D.A. Guidelines for the use and
Interpretation of Adsorption Isotherm Models: A Review. J.
&26] Kucherenko, V.O.; Tamarkina, Yu.V.; Popov, A.F. Luzhna
actyvatsiva z teplovym udarom – novyi sposib otrymannya
nanoporuvatyh vygletsevyh materialiv. Dopovidi Natsional'noi
Akademii Nauk Ukrayiny 2016, 12, 74-81.
https://doi.org/10.15407/dopovidi2016.12.074
[27] Chmiola, J.; Yushin, G.; Gogotsi, Y.; Portet, C.; Simon, P.;
Taberna, P.L. Anomalous Increase in Carbon Capacitance at Pore
Mzes Less Than 1 nanometer. Science 2006. 313, 1760–1763.
https://doi.org/10.1126/science.1132195
£28] Jiang, Y.; Chen, J.; Zeng, Q.; Zou, Z.; Li, J.; Zeng, L.; Sun,
W.; Li, C.M. Facile Method to Produce Sub-1 nm Pore-Rich
Carbon from Biomass Wastes for High Performance
Supercapacitors. Colloid Interface Sci. 2022, 612, 213–222.
https://doi.org/10.1016/j.jcis.2021.12.144
[29] Guerrera, J.V.; Burrow, J.N.; Eichler, J.E.; Rahman, M.Z.;
Mamireddy, M.V.; Friedman, K.A.; Coffman, S.S.; Calabro, D.C.;
Mullins, C.B. Evaluation of Two Potassium-Based Activation
Agents for the Production of Oxygen- and Nitrogen-Doped Porous
Carbons. Energy Fuels 2020, 34, 6101-6112.
https://doi.org/10.1021/acs.energyfuels.0c00427
[30] Zhang, Y.; Peng, J.; Feng, G.; Presser, V. Hydration Shell
Energy Barrier Differences of Sub-Nanometer Carbon Pores
Enable Ion Sieving and Selective Ion Removal. Chem. Eng. J.
2021, 419, 129438. https://doi.org/10.1016/j.cej.2021.129438
[B1] Deditius, A.; Ela, W.P.; Wiśniewski, M.; Gauden, P.A.;
Terzyk, A.P.; Furmaniak, S.; Włoch, J.; Kaneko, K.;
Neimark, A.V. Super-Sieving Effect in Phenol Adsorption from
Aqueous Solutions on Nanoporous Carbon Beads. Carbon 2018,
#35, 12–20. https://doi.org/10.1016/j.carbon.2018.03.063
[32] Chen, C.; Geng, X.; Huang, W. Adsorption of 4-
Chlorophenol and Aniline by Nanosized Activated Carbons.
h
a
```

8Y 20 21

```
Chem. Eng. J. 2017, 327, 941-952.
https://doi.org/10.1016/j.cej.2017.06.183
[33] Ahmed, M.J.; Theydan, S.K. Adsorption of p-Chlorophenol
onto Microporous Activated Carbon from Albizia Lebbeck Seed
Pods by One-Step Microwave Assisted Activation. J. Anal. Appl.
Pyrolysis 2013, 100, 253-260.
https://doi.org/10.1016/j.jaap.2013.01.008
[34] Wu, F.-C.; Wu, P.-H.; Tseng, R.-L.; Juang, R.-S. Preparation
of Activated Carbons from Unburnt Coal in Bottom Ash with
KOH Activation for Liquid-Phase Adsorption. J. Environ.
Manage. 2010, 91, 1097-1102.
https://doi.org/10.1016/j.jenvman.2009.12.011
J
§36] Dao, M. U.; Le, H. S.; Hoang, H. Y.; Tran, V. A.; Doan, V.
D.; Le, T. T. N.; Sirotkin, A. Natural Core-Shell Structure
Activated Carbon Beads Derived from Litsea glutinosa Seeds for
Removal of Methylene Blue: Facile Preparation, Characterization,
and Adsorption Properties. Environ. Res. 2021, 198, 110481.
Kttps://doi.org/10.1016/j.envres.2020.110481
A
В
[38] Li, L.; Wu, M.; Song, C.; Liu, L.; Gong, W.; Ding, Y.;
Nao, J. Efficient Removal of Cationic Dyes via Activated Carbon
with Ultrahigh Specific Surface Derived from Vinasse Wastes.
Bioresour. Technol. 2021, 322, 124540.
https://doi.org/10.1016/j.biortech.2020.124540
£39] Asuguo, E.; Martin, A.; Nzerem, P.; Siperstein, F; Fan, X.
Adsorption of Cd (II) and Pb (II) Ions from Aqueous Solutions
Using Mesoporous Activated Carbon Adsorbent: Equilibrium,
A
S
J
a
W
dLow-Cost Activated Carbon Preparation from Corn stigmata
Fibers Chemically Activated Using H<sub>3</sub>PO<sub>4</sub>, ZnCl<sub>2</sub> and KOH:
Study of Methylene Blue Adsorption, Stochastic Isotherm and
Ħ
ç
A
h
O
K
h
m
a
ħ
c
Z
A
2
```

Kinetics and Characterisation Studies. *J. Environ. Chem. Eng.* 2017, *5*, 679–698. https://doi.org/10.1016/j.jece.2016.12.043 [40] Ghorbani, M.; Seyedin, O.; Aghamohammadhassan, M. Adsorptive Removal of Lead (II) Ion from Water and Wastewater Media Using Carbon-Based Nanomaterials As Unique Sorbents: A Review. *J. Environ. Manage.* 2020, *254*, 109814. https://doi.org/10.1016/j.jenvman.2019.109814 [41] Jiang, J.; Li, R.; Yang, K.; Li, Y.; Deng, L.; Che, D. Investigation on Pb²⁺ Adsorption Characteristics by AAEMs-Rich Biochar in Aqueous Solution: Performance and Mechanism. *Environ. Res.* 2023, *236*, 116731. https://doi.org/10.1016/j.envres.2023.116731 [42] Mahadevi, A.S.; Sastry, G.N. Cation-π Interaction: Its Role and Relevance in Chemistry, Biology, and Material Science. *Chem. Rev.* 2013, *113*, 2100–2138.

Received: November 10, 2024 / Revised: February 09, 2025 / Accepted: February 15, 2025

ПОРИСТА СТРУКТУРА Й АДСОРБЦІЙНІ ВЛАСТИВОСТІ АКТИВОВАНОГО ВУГЛЕЦЮ НА ОСНОВІ ВУГІЛЛЯ, ОТРИМАННОГО ЛУЖНОЮ АКТИВАЦІЄЮ З ТЕРМОУДАРОМ

Анотація. Уперше досліджено адсорбцію фенолу, 4-хлорфенолу, метиленового блакитного та Pb(II) зразками активованого вуглецю, отриманими лужною активацією з термоударом. Виміряно кінетику й ізотерми адсорбції та порівняно з аналогічними даними для вуглецю, отриманого температурно-програмованою активацією. Визначено, що швидкість адсорбції лімітується взаємодією адсорбату з поверхневими центрами, а не дифузією до пор. Термоудар збільшує швидкості адсорбції в 1,18 — 3,16 рази, а рівноважну ємність — в 1,13 — 2,08 рази залежно від адсорбату і типу вугілля. Зразки вуглецю, отримані термошоком, є ефективнішими адсорбентами для очищення води від екотоксикантів.

Ключові слова: вугілля, лужна активація, термоудар, активоване вугілля, адсорбція, екотоксикант.